

Biocompatible L-Cysteine Capped MoS₂ Nanoflowers for Antibacterial Applications: Mechanistic Insights

Rupal Kaushik¹, Suwendu Nandi², Mahitosh mandal², Amar Nath Gupta^{1*}

¹ Soft Matter and Biophysics Laboratory, Department of Physics, IIT Kharagpur, 721302, India

²Cancer Biology Laboratory, School of Medical Science and Technology, IIT Kharagpur, 721302, India

* Corresponding author, *Email address:* ang@phy.iitkgp.ac.in (Amar Nath Gupta)

Abstract:

The development of multi-drug-resistant bacterial infections seriously threatens public health, so efforts are needed to develop a new class of safe and effective antibacterial agents. Here, we report a bio-inspired synthesis of surface-modified MoS₂ Nanoflowers with L-cysteine (MoS₂-cys NFs) that show good colloidal stability in an aqueous medium. The FE-SEM and TEM data confirm the flower-like morphology and determine the size of NFs (537± 12 nm); the XRD data predicts the hexagonal crystal structure of the NFs. The XPS peaks confirm the formation of MoS₂ NFs with surface modification by L-cysteine. FTIR measurements also confirm the presence of L-cysteine in the NFs. The antibacterial activity of as-prepared MoS₂-cys NFs examined over gram-negative *Escherichia coli* and gram-positive *Staphylococcus aureus* bacteria shows inhibition of nearly 97% and 90%, respectively, at concentrations 250 µg/mL each after incubation of 6 hrs. The antibacterial mechanism is mainly attributed to the generation of oxidative stress, which can occur through both ROS-dependent and ROS-independent pathways. The ROS-dependent and ROS-independent oxidative stresses were measured using flow cytometry and fluorescence imaging using DCFH-DA staining, and Ellman's assay, respectively. Moreover, the toxicity studies of the MoS₂-cys NFs towards HFF cell lines suggested the high biocompatibility of the nanomaterial with a cell viability of nearly 90%. We report the intrinsic antibacterial efficiency of MoS₂-cys NFs without any external stimulus (light, H₂O₂, etc.), doping, or drug loading. Our study indicates that the proper surface modification can enhance the colloidal stability and antibacterial potency

of MoS₂-based nanomaterials for further applications such as antibacterial coatings, water disinfection, and wound healing.

Keywords: MoS₂, L-cysteine, antibacterial, ROS (Reactive oxygen species), oxidative stress, toxicity, colloidal stability.

1. Introduction:

Microbial infections are one of the major threats to human health, accounting for millions of deaths worldwide¹. Antibiotics have traditionally been used to treat these infections. However, overuse of these traditional antibiotics is leading to the development of antimicrobial resistance^{2,3}. Therefore, there is an urgent need to design and develop novel antibacterial agents to address this problem. Recently, substantial efforts have been made to develop the potential nanomaterial-based antibiotics to counter multidrug-resistant infections and improve their antibacterial efficiency^{4,5}. In this context, silver nanoparticles have been extensively studied and applied as antimicrobial agents for water purification, wound healing, and antibacterial coatings in the textile and food packaging industries⁶. Despite this, their potential as antibacterial drugs is constrained by their toxicity to the host⁷. Antibiotics based on gold nanoparticles have also demonstrated effectiveness against multidrug-resistant bacteria⁸. Beyond metal nanoparticles, two-dimensional (2-D) nanomaterials have also emerged as promising antibacterial agents in the last decade⁹.

In this category, a 2-D nanomaterial Molybdenum disulfide (MoS₂), in particular, has earned significant attention due to its remarkable properties such as high catalytic activity, biocompatibility, low cost, ease of synthesis, and large surface area, hence its ability to communicate more with different biomolecules¹⁰. These properties have led to their use in various biomedical applications such as water disinfection, drug delivery, phototherapy, biosensing, antibacterial and anticancer agents, and wound healing^{11,12}. The nanostructures have great potential

as antibacterial agents, but their aggregation limits their biomedical applications. Yang et al. recently reported the stable dispersions of chemically exfoliated MoS₂ nanosheets (NSs) had shown nearly double antibacterial activity than the aggregated sheets due to their greater interaction abilities with the bacteria¹³. Hence, their study suggests that aggregating MoS₂ nanostructures in an aqueous medium decreases their antibacterial efficiency. Therefore, for MoS₂ to truly realize its full potential in biological applications, its surface must be appropriately modified to avoid aggregation and improve its solubility in aqueous media. Various reports suggest that the surface modification of nanoparticles with a nature motif may improve their interactions with biosystems, biocompatibility and increase their solubility in the aqueous medium^{14,15}.

L-cysteine, a hydrophilic sulfur-containing semi-essential amino acid, is extensively used to synthesize different cysteine-capped nanomaterials¹⁶⁻¹⁹. L-cysteine is a biocompatible, easy-to-obtain, environment-friendly, and inexpensive biomolecule. Moreover, its ability to coordinate with inorganic cations and metals via its three active functional groups (-NH₂, -COOH, and -SH) makes it an ideal capping agent and a greener sulfur source^{20,21}. The cysteine-capped nanostructures increase the aqueous stability and anchor other molecules due to the free amino and carboxyl groups on their surfaces²¹. These studies make L-cysteine a suitable ligand for synthesizing nanomaterials for various applications. Recently, various studies have also reported the synthesis of cysteine-modified MoS₂ nanostructures for different biomedical applications²²⁻²⁴. Furthermore, the previous reports also suggest that L-cysteine exhibits antibacterial activity, due to which they have been applied on multiple fabrics for durable antibacterial properties^{25,26}. Also, the distinct antibacterial activities of D-cysteine and L-cysteine on different bacterial strains have been reported²⁷.

Various studies have been conducted so far based on MoS₂ nanocomposites in order to enhance their antibacterial properties. The majority of these works are focussed on the use of thiolated surfactants and ligands for functionalization^{28,29}, introducing doping elements³⁰, loading drugs/antimicrobial peptides onto the nanomaterial^{31,32}, and combining it with other nanomaterials like silver, ZnO, TiO₂ etc³³⁻³⁵. Moreover, photothermal, photodynamic, photocatalytic properties, and peroxidase like activities of MoS₂ have led to development of synergistic external stimuli responsive antibacterial system with enhanced antibacterial efficiency of the MoS₂-based nanocomposites³⁶⁻⁴⁰. Zhao et al. reported the synergistic antibacterial activity of NIR-assisted streptomycin sulfate loaded PEG-MoS₂/reduced graphene oxide (PEG-MoS₂/rGO-SS) nanoflakes. The results reveals that, the antibacterial activity of PEG-MoS₂ alone is very feeble as compared to PEG-MoS₂/rGO-SS nanoflakes both with and without NIR treatment³⁷. Hence, it was found in all aforementioned studies that MoS₂ nanostructures alone (without functionalisation, drug loading, or external stimuli) have shown very low antibacterial activity as compared to the whole nanocomposite.

Moreover, MoS₂ nanoflowers (NFs) are gaining attention due to their unique flower-like morphology consisting of many NSs stacked in a three-dimensional (3D) nanostructure to provide greater surface area and more active edges than their 2D NSs¹². It is expected that due to more active sites, NFs will possess good antibacterial activity. Recently, polyethylene glycol (PEG) functionalized MoS₂ NFs have shown negligible antibacterial activity in absence of H₂O₂ and NIR irradiation³⁶. To the best of our knowledge, research based on MoS₂ NFs is still in the infant stage for antibacterial applications. Very few reports are there, based on surface-modified MoS₂ NFs, exploring their intrinsic antibacterial properties without any drug loading or external probes. In

addition to this, limited studies have reported the colloidal stability of as-synthesised nanostructures.

Hence, in this work, we synthesized L-cysteine-capped MoS₂ NFs using facile hydrothermal synthesis method. The as-synthesised MoS₂-cys NFs have shown good antibacterial activity, with 97 % and 90 % inhibition against *E. coli* (gram-negative) and *S. aureus* (gram-positive) bacteria, respectively, at 250 µg/mL and 6 hours of incubation. The MoS₂-cys NFs are highly stable in aqueous solution, as shown through microplate reader and DLS measurements. Moreover, as-synthesized MoS₂-cys NFs confirm the high biocompatibility through cellular toxicity studies towards HFF cell lines. To better understand the antibacterial mechanism, flow cytometry and fluorescence imaging via DCFH-DA staining and GSH oxidation assays were performed to determine ROS-dependent and ROS-independent oxidative stress, respectively, *in-vitro*. Therefore, the results suggest that the antibacterial activity of MoS₂-cys NFs over both bacterial strains is due to the combined effect of membrane rupture, ROS-dependent, and ROS-independent oxidative stresses. Hence, our study indicates that the as-synthesized MoS₂-cys NFs exhibits remarkable antibacterial properties, high colloidal stability, and favourable biocompatibility towards mammalian cells.

2. Experimental section:

2.1. Materials:

Sodium molybdate dihydrate (Na₂MoO₄·2H₂O, 99%), thiourea (NH₂CSNH₂, >99%), L-cysteine (HSCH₂CH(NH₂)CO₂H, >98.5%), were all purchased from Sigma-Aldrich. MTT (3-(4,5-dimethylthiazol-2-yl)-2,5-diphenyl tetrazolium bromide) reagent, Glutathione (GSH), and 5,5'-dithiobis(2-nitrobenzoic acid) (DTNB), and Luria-Bertani broth (LB) were acquired from Sisco Research Laboratories Pvt. Ltd. (SRL) India. Dimethyl sulfoxide (DMSO), Hydrogen Peroxide

(H₂O₂), Phosphate-buffered saline (PBS, PH \approx 7.4), DCFH-DA (2',7'-Dichlorofluorescein diacetate), were purchased from Sigma-Aldrich.

2.2. Synthesis of MoS₂-cys NFs:

The MoS₂-cys NFs were synthesized using a previously reported method with some modifications²⁴. Briefly 0.01M of Na₂MoO₄·2H₂O was dissolved in 55 ml of Deionized (DI) water, followed by 45 minutes of stirring. Subsequently, 0.01M L-cysteine was introduced into the solution and stirred for another 45 minutes. Then, thiourea (2:1) was slowly added to the solution, and the mixture was again stirred for another 30 mins. Then, the obtained solution was transferred into a 100 ml Teflon-lined stainless-steel autoclave and heated at 200 °C for 24 hrs. After allowing the autoclave to cool, the suspension was washed several times with DI water and absolute ethanol, respectively. Finally, after vacuum drying, we obtained MoS₂-cys NFs. The schematic of the synthesis process is shown in Fig.1

2.3. Characterisation of MoS₂-cys NFs:

The X-ray diffraction (XRD) analysis was conducted using the X'Pert Pro high-resolution X-ray diffractometer (Philips PANalytical). The measurements were taken within the 2 θ angle range of 10° to 70°, using Cu K α radiation (λ =1.5406 Å). The size and morphology of the particles were determined using Field Emission-Scanning Electron Microscopy (FE-SEM, CARL ZEISS SUPRA 40, 20 kV) equipped with Energy Dispersive X-ray (EDX), and transmission electron microscopy (TEM, FEI-TECNAI G220S-Twin operated at 200 kV). X-ray photoelectron spectroscopy (XPS) measurements with a monochromatic Al-K α source were recorded under high vacuum conditions using a PHI-5000 VERSA Probe II, Inc., Japan. Fourier Transform infrared (FTIR) spectroscopy measurements were done using Thermofisher Scientific Instruments, USA, Model: Nicolet 6700. The thermogravimetry analysis (TGA) was done using a PerkinElmer

Diamond TG/DTA thermal analyzer at a heating rate of 10 °C/min from 25 °C to 750 °C under an air atmosphere. The colloidal stability studies were done using a microplate reader (BioRad, iMark, Japan) by measuring optical density (OD) value at wavelength 595 nm and using a dynamic light scattering (DLS) experiment by measuring mean scattered light intensity from the sample at 90° with the help of Photocor complex, Photocor Ltd. Russia. The light source is a Ga-As diode laser at wavelength 653.8 nm and constant output power of 35 mW.

2.4. Assay for antibacterial activity of MoS₂-cys NFs:

An antimicrobial growth kinetics study examined the effect of as-synthesized MoS₂-cys NFs over bacterial growth. The two bacterial strains used in this study were gram-negative *E. coli* and gram-positive *S. aureus* bacteria. We incubated both bacterial cultures separately in fresh LB broth medium at 37 °C and 150 revolutions per minute for 16 hours. The bacterial inoculums were prepared (at 10⁷-10⁸ CFU/ml), cultured in 96 well plates, and treated with increasing concentrations of MoS₂-cys NFs from 31.25 µg/ml to 250 µg/ml against both *E. coli* and *S. aureus* bacteria separately. Here, the inoculum with fresh LB medium and bacteria (non-treated) was considered the negative control. The effectiveness of the treatment was determined by establishing the growth curve of bacteria by measuring the OD value at 595 nm using a microplate reader (BioRad, iMark, Japan) every 30 minutes for 6 hours. The results were also given as the inhibition percentage of treated cell growth compared to the growth of negative control (not treated) cells. The following equation can estimate the percentage inhibition:

$$\% \text{ Inhibition} = \frac{\text{OD}_{\text{control}} - \text{OD}_{\text{treated}}}{\text{OD}_{\text{control}}} \times 100 \quad (1)$$

2.5. Intracellular ROS detection Assay:

The amount of intracellular ROS in bacterial cells was determined by following a specific ROS detection assay using flow cytometry and fluorescence imaging using a fluorescent probe DCFH-DA⁴¹. In this study, *E. coli* and *S. aureus* were allowed to grow in an incubator overnight at 37 °C. The cells were then treated with MoS₂-cys NFs at concentrations of 62.5 µg/mL and 250 µg/mL at 10⁷-10⁸ CFU and kept at 37 °C. An untreated sample was used as a negative control for each bacterial strain. After 6 hours of treatment, cell pellets were collected by centrifugation at 11,000 rpm for 10 min and washed thrice with PBS. The cells were then stained with 10 µM of DCFH-DA solutions and incubated at 37 °C for 30 min in the dark. The production of ROS in the cells in response to MoS₂-cys NFs was analyzed by imaging using fluorescence microscopy at 40X magnification (Nikon eclipse, Ts2R). Another set-up for flow cytometry analysis is prepared in the same way to quantify the level of cellular oxidative stress triggered by increasing dosages (62.5 and 250 µg/mL) of MoS₂-cys by measuring fluorescence intensity using flow cytometry (BD LSRFortessa™).

2.6. Ellman's assay: GSH oxidation test

The loss in GSH activity is well determined using Ellman's assay according to previously reported protocol¹³. For this study, MoS₂-cys NFs were diluted in 50 mM bicarbonate buffer (of pH 8.6) to a concentration of 31.25 µg/mL, 62.5 µg/mL, 125 µg/mL, 250 µg/mL, 500 µg/mL, and 1 mg/mL. With the dilutions, GSH (0.8 mM) was added to the microcentrifuge tube to initiate the oxidation process. H₂O₂ (1 mM) was a positive control, while GSH (0.8 mM) was the negative control. The mixture was subsequently covered with alumina foil to prevent light exposure and placed in a shaker at room temperature at 150 rpm for 2 and 4 hours, respectively. After incubation, 0.05 M Tris-HCl and 100 mM DTNB (Ellman's reagent) were added to the mixture. A syringe

filter (0.22 μm membrane filter) was used to filter the MoS₂-cys NFs from the mixture. A 96-well plate was loaded with 100 μL aliquots of the filtered solution. The absorbance was then determined at 412 nm using the microplate spectrophotometer (BioRad, iMark, Japan). The equation estimates the percentage loss of GSH:

$$\% \text{ Loss of GSH} = \left(1 - \frac{\text{OD}(\text{treated with NFs})}{\text{OD}(\text{untreated})} \right) \times 100 \quad (2)$$

2.7. Cellular toxicity studies:

The cytotoxicity of MoS₂-cys NFs was estimated on a normal human foreskin fibroblast (HFF) cell line, *in-vitro*. In a 96-well plate, 2.96×10^6 normal HFF cells were plated and allowed to attach in an incubator for 24 hours. After 24 hours, the cells were treated with a serum-free medium supplemented with different concentrations of MoS₂-cys NFs and incubated for 48 hours. After 48 hours of incubation, cells were assessed by the 3-(4,5-dimethylthiazol-2-yl)-2,5-diphenyl tetrazolium bromide (MTT, Sigma Aldrich, USA) assay protocol. The optical density was taken using a microplate spectrophotometer (BioRad, iMark, Japan) at 595 nm, and the results were analyzed. Cell viability was determined using the following formula:

$$\text{Cell viability} = \frac{\text{Absorbance of treated HFF cells}}{\text{Absorbance of the control cells}} \times 100$$

3. Results and Discussion:

3.1. Synthesis and characterization of MoS₂-cys NFs:

The L-cysteine-capped MoS₂ NFs were successfully synthesized using a hydrothermal process. The reaction mechanism in Fig.1 shows that initially, during the crystallization process, MoS₂ NSs

are formed. Then, the edge-to-edge, edge-to-surface, and few surface-to-surface attachments during the reaction led to the formation of the NFs³¹.

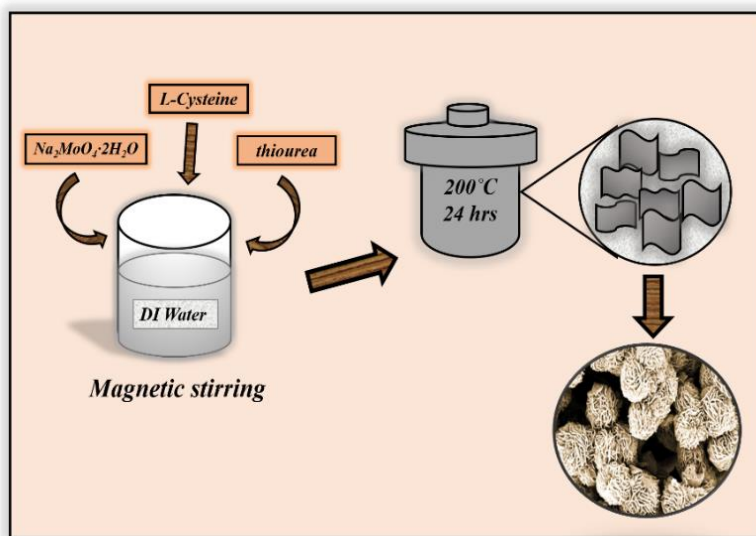


Figure 1. Schematic representation of the synthesis process and growth mechanism of MoS₂-cys NFs

The morphology and size of the as-obtained MoS₂-cys NFs were validated using FE-SEM and TEM. SEM image (Fig. 2a) shows the flower-like morphology of cysteine-capped MoS₂ nanostructures with plenty of edges. It can be observed that the NFs are composed of MoS₂ NSs arranged in the form of petals. The greater surface area and more edges in the NFs will help in more significant interaction of NFs with the bacteria and hence, may help increase the antibacterial activity⁴². The mean size of obtained NFs is 537± 12 nm, as calculated using the particle distribution curve in Fig. 2b.

The TEM images (Fig. 2c and S3) show that NFs are made up of few-layer MoS₂ NSs closely packed to form a flower-like structure. The EDX Spectrum (Fig.S1) and Elemental mapping analysis (Fig.S2) confirm the uniform distribution of Mo, S, C, N, and O among MoS₂-cys NFs.

The above results suggest that the prepared nanostructures could be MoS₂ NFs capped by L-cysteine.

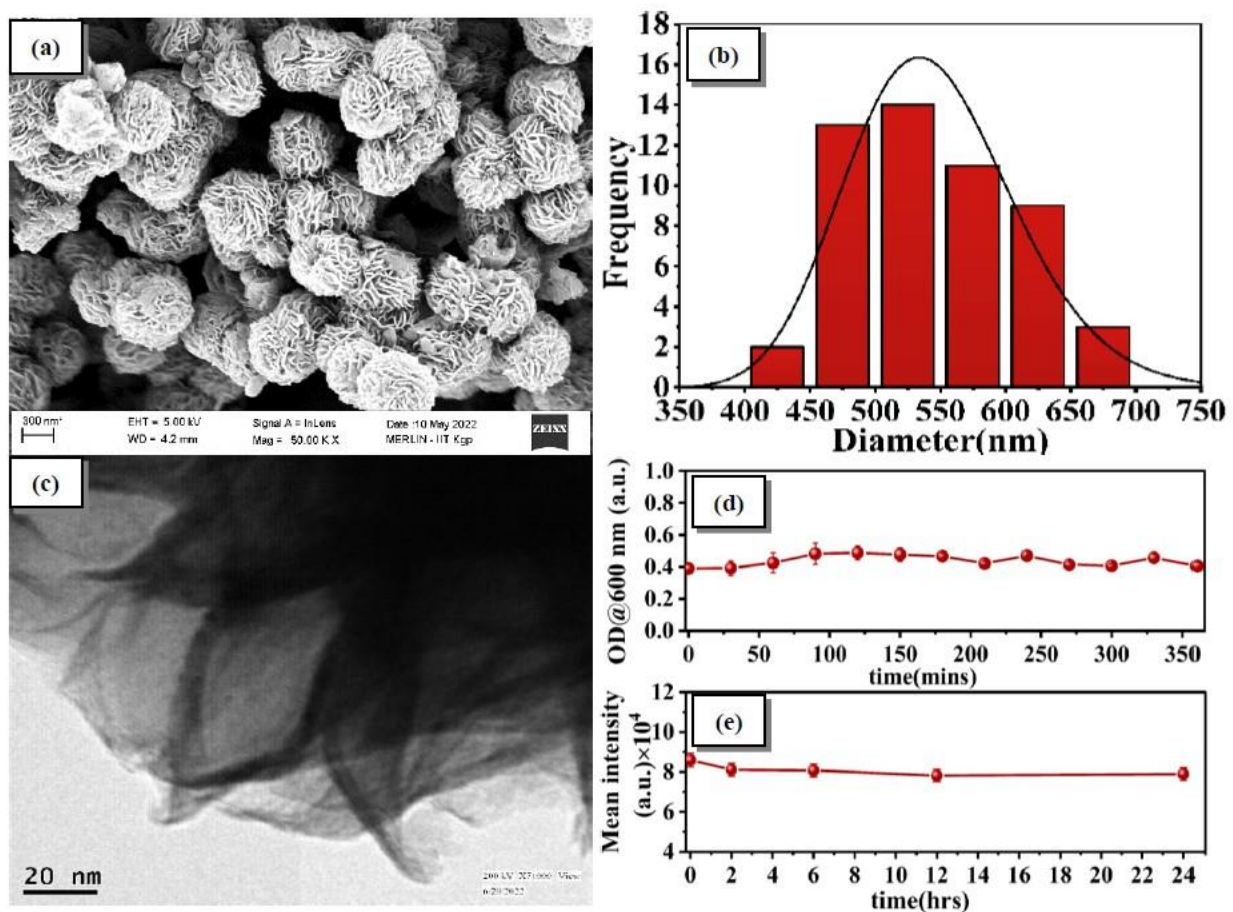


Figure 2. Morphology characterizations and colloidal stability of MoS₂-cys NFs, (a) SEM image of MoS₂-cys NFs, (b) corresponding size distribution, (c) TEM images of MoS₂-cys NFs, and (d & e) colloidal stability measurements of MoS₂-cys NFs using optical density values and mean scattered intensity, respectively with time

Further, Fig. 2d and 2e represent the colloidal stability studies of MoS₂-cys NFs using the OD values and the mean scattered intensity measurements, respectively. The previous studies found that aggregation of MoS₂ reduces its antibacterial effectiveness^{13,43}. Hence, first using a microplate reader, OD values of the NFs at the concentration of 250 µg/ml are measured. The stability is

investigated for the duration at which experimental studies for antibacterial activities are being performed. The increase in OD values usually indicates aggregation or poor stability of the complexes⁴⁴. But, Fig. 2d shows that the OD value increases only nearly 2 % after 6 hours of incubation at 37°C. Therefore, the results suggest that the stability of the MoS₂-cys NFs is not affected during experimental conditions.

Moreover, the colloidal stability of nanoparticles is also assessed by measuring the mean scattered intensity from the NFs using DLS. The reduction in mean intensity indicates, aggregation of nanoparticles due to which they settle down. Fig. 2e shows only a 3 % decrease in intensity indicating minimal aggregation of nanoparticles even after 24 hours of incubation. These findings suggests the good colloidal stability of the MoS₂-cys NFs. However, it is known that the nanoparticles have a tendency to aggregate. But, their aggregation can be minimized with proper surface modification. Fig. S4 illustrates only 30 % of aggregation, even after 28 days of incubation. Hence, the above results reveals that the as-synthesized MoS₂-cys NFs are highly stable in aqueous media.

The possible crystal structure of as-prepared MoS₂-cys NFs was determined by analyzing the XRD pattern. From Fig.2, the diffraction peaks of the MoS₂-cys NFs correspond to (002), (100), (101), (006), (105), (110), and (008) lattice planes. These diffraction peaks could be indexed to the hexagonal structure of MoS₂ (JCPDS No. 37-1492). No other impurity peaks appeared in the XRD pattern, indicating that the formed MoS₂-cys structures are highly pure. The broadening of diffraction peaks suggests that the ultrathin dimensions of MoS₂ NSs in the NFs, which aligns with the observations from TEM images²⁴. The crystallite size is found to be 2.02 nm, calculated using the standard Debye Scherrer formula.

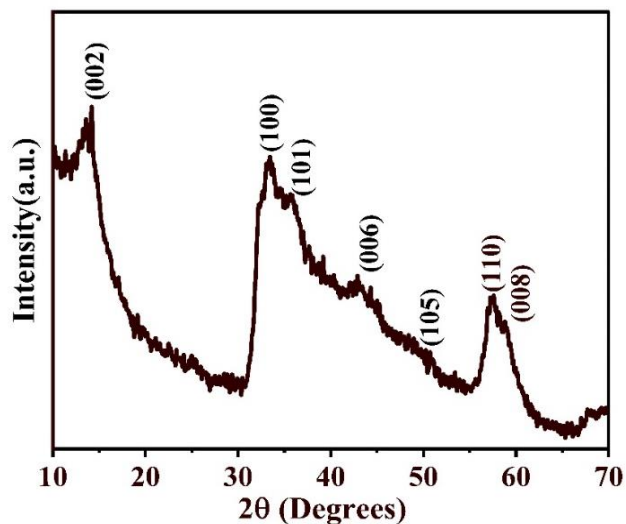


Figure 3. XRD spectra of MoS₂-cys NFs

The XPS was used to investigate the chemical composition and valence states of the synthesized MoS₂-cys NFs. The broad XPS spectrum is shown in Fig. 4a, which confirms the presence of Mo, S, C, and O in the synthesized sample. The high-resolution XPS spectrum of Mo and S is shown in Fig. 4b and c, respectively, as shown in the Mo 3d XPS spectrum of MoS₂-cys NFs, the two peaks at 229.2 eV and 232.4 eV can be assigned to Mo 3d_{5/2} and Mo 3d_{3/2} modes of 2H-MoS₂ in the Mo⁴⁺ valence state^{13,45}.

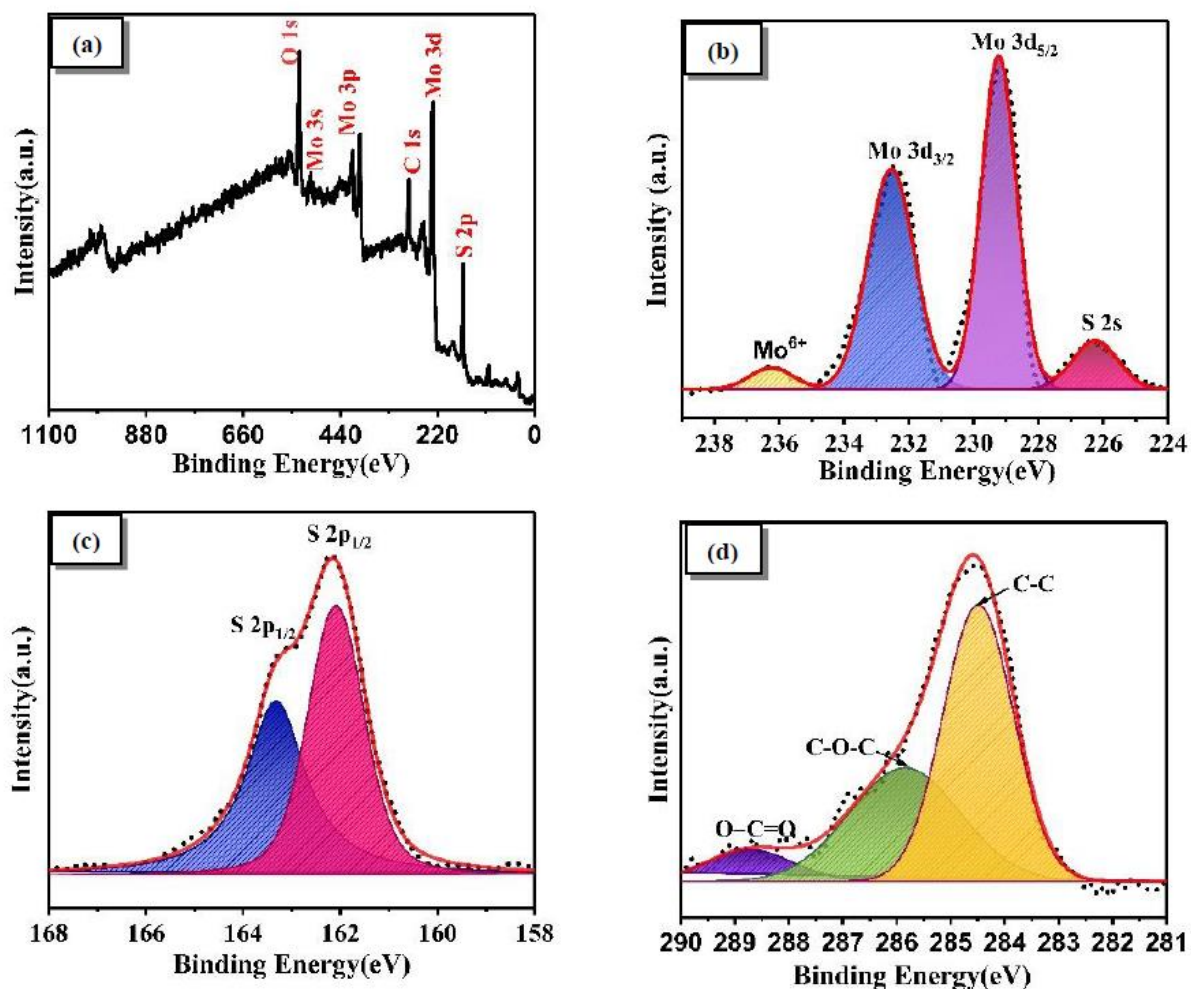


Figure 4. XPS spectra of MoS₂-cys NFs, (a) complete XPS scan of MoS₂-cys NFs (b) XPS spectra of Mo 3d, (c) XPS spectra of S 2p, and (d) XPS Spectra of C 1s.

Additionally, there is a small peak at 236.1 eV, which corresponds to the Mo⁶⁺ valence state of Mo. Further, one small peak at 226.3 eV corresponds to S 2s. Similarly, the characteristic peak at 162.1 eV and 163.2 eV corresponds to the S 2p_{3/2} and S 2p_{1/2} corresponding to the S²⁻ valence state of the sulfur element^{13,24}. These results indicate the formation of MoS₂. Fig. 3d shows the High-resolution XPS C 1s spectrum where three peaks appeared at 284.5 eV (C-C), 285.85 eV (C-O-C/C-OH), and 288.86 eV (O-C=O)^{46, 47}. These peaks may be due to the presence of cysteine over the surface of MoS₂-cys NFs. Further, FTIR measurements were done to verify the presence of L-

cysteine in MoS₂-cys NFs. FTIR spectrum of MoS₂-cys NFs and L-cysteine is shown in Fig. 5a. In FTIR spectra of L-cysteine, the main absorption bands at 1606 and 1389 cm⁻¹ can be assigned to asymmetric and symmetric stretching of COO⁻, 2545 cm⁻¹ corresponding to S-H^{20,48}, and 2074 cm⁻¹ to C-H vibrations. Moreover, the band at 1525 cm⁻¹ corresponds to the N-H vibrations²⁰, 1054 cm⁻¹ to NH₃ rocking, and 1192 cm⁻¹ corresponds to CH₂ twisting⁴⁹. The absorption band from 3200 to 3500 cm⁻¹ belongs to the O-H group. This spectrum matches well with that of standard amino acids²⁰. Whereas in MoS₂-cys NFs, the spectrum clearly shows the distinctive peaks of Mo-O and Mo-S vibrations at around 600 and 481 cm⁻¹, respectively, corresponding to MoS₂, and the O-H stretching peak was found to be over 3330 to 3630 cm⁻¹ due to the absorption of atmospheric moisture by KBr⁴⁶. Moreover, the signature peaks of L-cysteine in the MoS₂-cys NFs with reduced absorbance compared to L-cysteine are clearly visible. While the absorption band of COO⁻ is shifted from 1606 to 1597 cm⁻¹ and from 1389 to 1397 cm⁻¹. Also, the peaks corresponding to C-H and S-H vibrations diminished in the NFs²⁰. These results indicate the effective binding of L-cysteine with MoS₂.

The TGA curves of MoS₂-cys NFs and L-cysteine are shown in Fig. 5b. In the curve of MoS₂-cys NFs, the initial 2.85 % weight loss of NFs is due to evaporation of water from the complex and 18.78% weight loss from 100 °C to 750 °C in the TGA curve of NFs can be assigned to the thermal decomposition of L-cysteine²⁴. Therefore, it shows that the amount of L-cysteine present in MoS₂-cys NFs is 18.78 %. The above results indicated the successful synthesis of the MoS₂-cys complex.

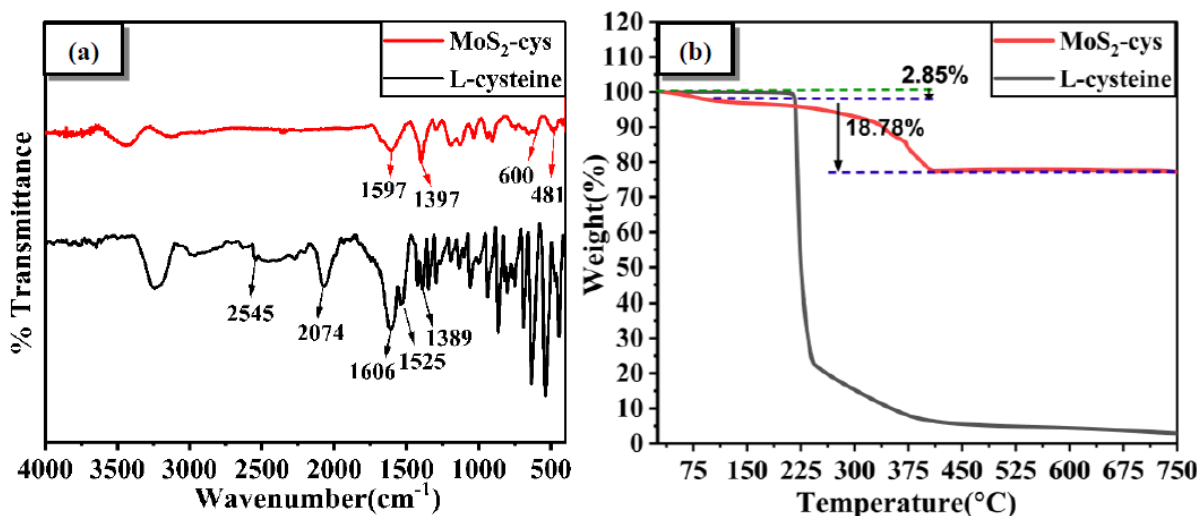


Figure 5. (a) FTIR spectra of MoS₂-cys NFs and (b) TGA curves of cysteine, and MoS₂-cys NFs

3.2. Antibacterial activity:

A bacterial growth kinetics study investigated the antibacterial activity of MoS₂-cys NFs against both Gram-negative *E. coli* and Gram-positive *S. aureus* bacteria. Both *E. coli* and *S. aureus* bacteria were exposed to MoS₂-cys NFs at varying concentrations. The growth curves demonstrate that the antibacterial activity of MoS₂-cys NFs against both the bacterial strains is concentration as well as time-dependent (Fig. 6a and 6b).

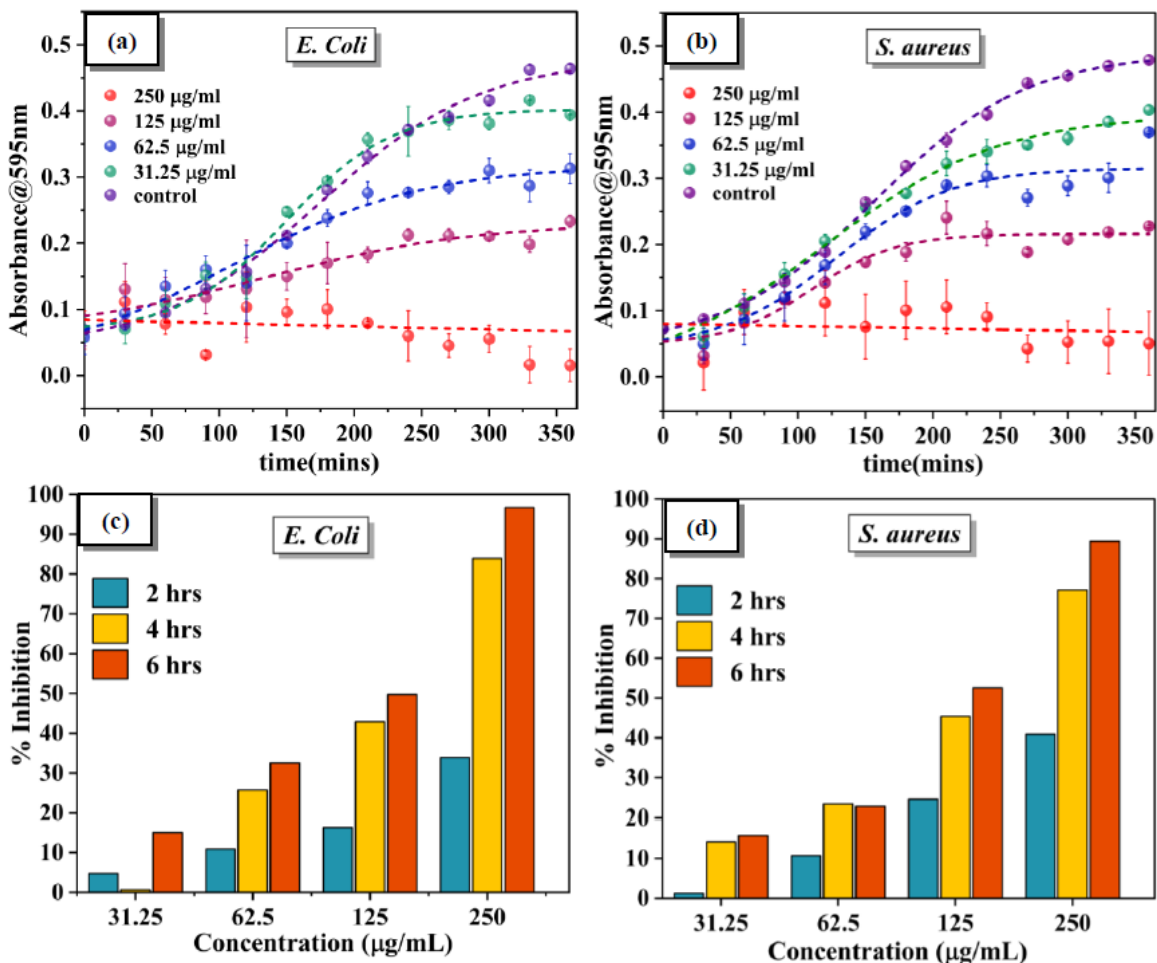


Figure 6. Antibacterial activity of MoS₂-cys NFs. Growth kinetics of (a) *E. coli* and (b) *S. aureus* treated with different concentrations of MoS₂-cys NFs (n=3, ***P<0.001 is relative to control). % Inhibition of (c) *E. coli* and (d) *S. aureus* treated with different concentrations of MoS₂-cys NFs.

The percentage inhibition of treated cells relative to the control is plotted in Fig. 6 c and d to estimate the antibacterial activity of MoS₂-cys NFs. These results indicate that MoS₂-cys NFs have significantly reduced bacterial growth in both concentration- and time-dependent manner. After 6 hours of treatment, the MoS₂-cys NFs were found to inhibit the growth of *E. coli* by approximately 50 % at a concentration of 125 µg/mL which was increased to 97% at a concentration of 250 µg/mL. Moreover, the antibacterial efficiency of MoS₂-cys NFs against *E. coli* increased from 84% (after 4 hrs) to 97% (after 6 hrs) at a concentration of 250 µg/mL, indicating that this concentration

of MoS₂-cys NFs is most effective in inhibiting the growth of Gram-negative bacterial cells (Fig. 6c).

Similar, antibacterial activities were also observed against the *S. aureus* bacteria, exhibiting a dependence on both concentration and time. However, at 250 µg/mL concentrations, *S. aureus* inhibition is nearly 75 % after 4 hours and almost 90 % after 6 hours. As a result, when compared to *S. aureus*, MoS₂-cys NFs were found to be more efficient at preventing the growth of *E. coli*. (Figure 6d.). A thick peptidoglycan layer surrounding gram-positive bacterial cells could explain the relatively less effectiveness of MoS₂-cys NFs in inhibiting the growth of *S. aureus* compared to *E. coli*⁵⁰.

Study	Nanostructures	Incubation period (hours)	Light irradiation	Antibacterial activity %				Colloidal stability	References
				With light		Without light			
				<i>E. Coli</i>	<i>S. aureus</i>	<i>E. Coli</i>	<i>S. aureus</i>		
Silver-Infused MoS ₂	1. Cys- MoS ₂ NSs (30 µg/mL) 2. Ag ⁺ -Cys-MoS ₂ NSs (30 µg/mL) 3. PDDA-Ag ⁺ -Cys-MoS ₂ NSs (15 µg/mL for <i>E. Coli</i> and 10 µg/mL for <i>S. aureus</i>)	8	-	-	-	1. none 2. 80% 3. 100%	1. none 2. nearly 60% 3. 100%	Not reported	33
PEG functionalized MoS ₂ /rNFs	1. PEG-MoS ₂ NFs (<i>E. Coli</i> at 100 and 1000 µg/mL) 2. PEG-MoS ₂ NFs+H ₂ O ₂ +light (<i>E. Coli</i> at 150 µg/mL)	12	808 nm laser irradiation (for 10 min)	1. - 2. 99%		1. none and 15% respectively 2. -	-	Not reported	36
PEG-MoS ₂ /rGO-SS nanoflakes	1. PEG-MoS ₂ 2. PEG-MoS ₂ /rGO 3. PEG-MoS ₂ /rGO-SS 4. PEG-MoS ₂ /rGO-SS + light	24	808 nm laser irradiation (for	4. 85%	4. 100%	1. 20% 2. 40% 3. 60% 4. -	1. 40% 2. 50% 3. 60% 4. -	Not reported	37

	(Both E. coli and S. aureus at concentration 150 µg/mL for all above)		30 min)						
MoS ₂ nanostructures	1. MoS ₂ NSs by ultrasonication 2. hydrothermally synthesized MoS ₂ NFs . 3. MoS ₂ NSs by lithium-ion intercalation (Conc. = 100 µg/mL)	3	White light LED irradiation(18 W for 3hrs)	1. 34% 2. 62% 3. 99%	-	1. 15% 2. 18% 3. 36%	-	Antibacterial efficiency is decreased significantly by greater than 10% after 3 rd cyclic antibacterial experiments	38
MoS ₂ NFs	1. 2H- MoS ₂ 2. 1T- MoS ₂ (Concentration= 0.4 mg/L)	3	Simulated solar AM1.5 light (for 4 mins)	1. 50% 2. 58%		1. no inhibition 2. 22%		Not reported	51
MoS ₂ QDs	1. MoS ₂ QDs 2. MoS ₂ NSs 3. Bulk MoS ₂ (Conc. = 50 µg/mL)	-	Simulated solar light (for 1 hour)	1.~50% 2.~90% 3. none	1. ~60% 2. ~90% 3. none	1.~20% 2. - 3. -	1. ~20% 2. - 3. -	Not reported	52
Amino acid functionalised MoS ₂ -QDS	1. MoS ₂ QDs (25 µg/mL) 2. phenylalanine functionalised MoS ₂ QDs 3. Leucine functionalised MoS ₂ QDs .	14	White light (30 min irradiation)	-	1. . ~30% 2. ~99% (at 0.62 µg/mL) 3. ~99% (at 4 µg/mL)	-	1. none (at 7 µg/mL) 2. ~99% (at 1.24 µg/mL) 3. ~99%	Not reported	53
MoS ₂ -Cys NFs (Our work)	MoS ₂ -Cys NFs: 1. 31.25 µg/mL 2. 62.5 µg/mL 3. 125 µg/mL 4. 250 µg/mL	6	-	-	-	1. 15% 2. 32% 3. 50% 4. 97%	1. 15% 2. 23% 3. 52% 4. 90%	Highly stable (~97% after 24 hours)	

Table 1. Antibacterial efficiency of different MoS₂ nanostructures

Therefore, the above-mentioned findings in the table demonstrate the enhanced antibacterial effectiveness is either through external functionalisation, light exposure and/or combination with other nanoparticles. Thus, our results indicate that even without the aid of external probes (like visible light, NIR light, etc.) or loading of any antibiotics/drugs, doping, or combination with any other nanomaterials, the as-synthesized MoS₂-cys NFs alone exhibits remarkable efficiency towards bacterial inhibition. Also, due to the photothermal property of MoS₂ nanostructures as mentioned above, we may also expect the further increase in antibacterial potential of MoS₂-cys NFs.

3.3. Mechanism of antibacterial action:

It has been reported that MoS₂-NSs can embed into the lipid layer by forming dents on the surface, causing the rupture of the lipid membrane, cytoplasm leakage, and, eventually, bacterial death⁵⁴. Moreover, the antibacterial mechanism of MoS₂-NSs by membrane depolarisation, bilayer disruption, oxidative stress, and metabolic inactivation has also been reported⁴⁰. Since MoS₂-NFs consist of several MoS₂-NSs, similar antibacterial mechanisms with improved antibacterial efficiency are expected due to presence of many active edges. Apart from membrane-directed bacterial death, oxidative stress plays a major role in the antibacterial action of MoS₂-NSs.

Typically, oxidative stress can arise in different ways. One is ROS-dependent oxidative stress. ROS are widely known to cause cell apoptosis and contribute to the antibacterial activity of various nanomaterials. During cellular metabolism, ROS is constantly generated⁵⁵. Even though bacteria have a defense system against ROS, excessive ROS will result in oxidative stress, destroying cellular components, including lipids, proteins, and nucleic acids, eventually killing the bacteria⁵⁶. Other, ROS-independent oxidative stress, in which nanomaterials disturb a specific microbial process by disrupting or oxidizing a critical cellular structure or component without generating

ROS¹³. We followed established protocols to determine the oxidative stress-mediated antibacterial mechanism of the MoS₂-cys NFs.

.3.1. Measurement of intracellular ROS:

First, we evaluated the possibility of ROS-generated oxidative stress by flow cytometry and fluorescence imaging using the DCFH-DA staining method. In the presence of ROS inside the cells, the non-fluorescent DCFH-DA dye is oxidized to form a green fluorescent molecule called dichlorofluorescein (DCF), which acts as the indicator of ROS⁴¹. Both the bacterial strains, *E. coli* and *S. aureus* were treated with different concentrations (0, 62.5, and 250 µg/mL) of MoS₂-cys NFs.

The results of flow cytometry-based ROS measurement clearly show a concentration-dependent ROS generation in both *E. coli* (Fig. 7a and S5) and *S. aureus* (Fig. 7b and S6) bacteria. In the case of *E. coli*, ROS generation is 52.5 % and 6 % after treatment with 250 µg/mL and 62.5 µg/mL concentrations of MoS₂-cys NFs, respectively, while the control only shows 0.7 % of ROS generation. While in the case of *S. aureus*, the ROS generation is 17.9 %, 2 %, and 0.54 % at the concentration of 250 µg/mL, 62.5 µg/mL, and 0 µg/mL (non-treated or control), respectively. The results also demonstrate that more ROS is generated in *E. coli* compared to *S. aureus*, which is consistent with the bacterial growth kinetics assay.

Further, fluorescence microscopy imaging using DCFH-DA staining was done to confirm the generation of ROS upon treatment with MoS₂-cys NFs. The intracellular ROS level is indicated by green fluorescence intensity⁵⁷. The results show that both *E. coli* (Fig. 7(c-e)) and *S. aureus*

(Fig. 7(f-h)) show enhanced green fluorescence and, thus, improved ROS production upon treatment with MoS₂-cys NFs as compared to their dark controls.

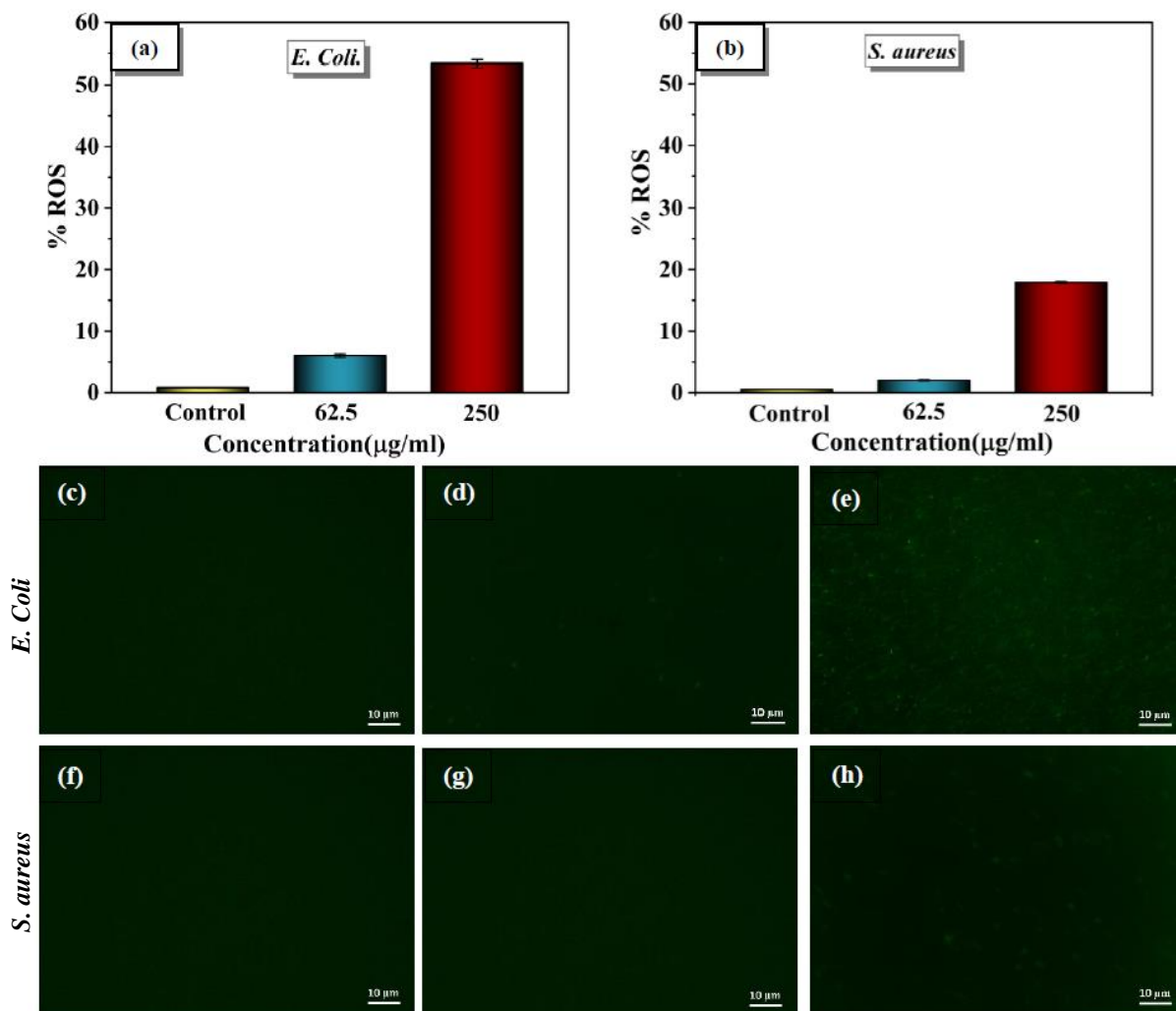


Figure 7. ROS generation at different doses of MoS₂-cys NFs. % ROS generation in (a) *E. coli*, and (b) *S. aureus* after treatment with different concentrations of MoS₂-cys NFs (n=3, ****P* < 0.001 relative to control). Fluorescence microscopy images of *E. coli* (c-e), and *S. aureus* (f-h) after exposure to 0 µg/mL (control) (c, f), 62.5 µg/mL (d, g), and 250 µg/mL (e, h) of MoS₂-cys NFs. (scale bar: 10 µm, Magnification: 40X).

Moreover, the fluorescent images show that the fluorescence intensity is dose-dependent, suggesting the dose-dependent ROS generation in both bacterial strains. Also, compared to *E. coli*, the ROS generation is less in *S. aureus*. These results are consistent with the flow cytometry

analysis as well as the bacterial growth kinetics study. The above results show ROS generation is a key factor in bacterial growth inhibition.

3.3.2. Loss in GSH activity:

Next, we investigated the possibility of ROS-independent oxidative stress using *in-vitro* GSH oxidation using Ellman's assay. GSH, a tripeptide that contains thiols, is present in the cells in large amounts in its reduced form, which spontaneously oxidizes upon exposure to molecular oxygen⁵⁸. As an antioxidant, it protects cells from oxidative stress. Excess ROS within cells causes oxidative stress and disrupts the equilibrium between pro-oxidants and antioxidants, oxidizing GSH into glutathione disulfide (GSSG). The oxidation of GSH to GSSG leads to a loss in GSH activity.

Consequently, GSSG cannot protect cells from oxidative damage, resulting in the oxidation of vital cellular components such as proteins, nucleic acids, lipids, etc., ultimately leading to the death of the cell⁵⁰. Ellman's assay can quantify the oxidative stress caused by GSH activity loss. In GSH oxidation experiments, bicarbonate buffer (50.0 mM at pH 8.6) without MoS₂-cys NFs and H₂O₂ (1.0 mM) were used as negative and positive controls, respectively.

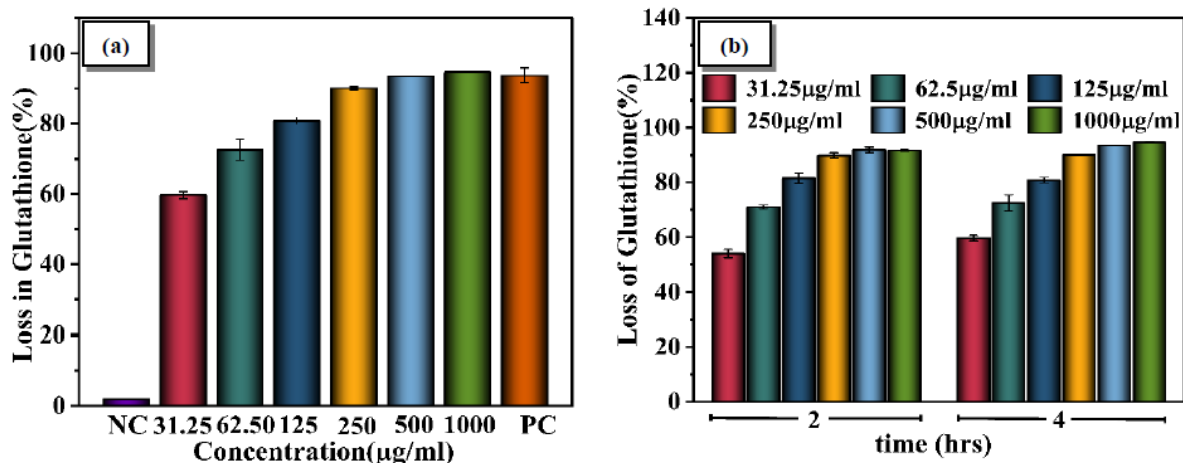


Figure 8. Oxidation of GSH by MoS₂-cys NFs. (a) Percentage loss of GSH after incubation with MoS₂-cys NFs dispersions of different concentrations for 4 h. H₂O₂ and bicarbonate buffer without NFs were used as positive and negative controls, respectively. (b) Time and concentration-dependent percentage loss of GSH. (n=3, ****P* < 0.001).

The objective of the negative control was to show that the incubation conditions did not cause GSH oxidation. The oxidation capacity of the MoS₂-cys NFs toward GSH showed a clear dependence on their concentration but no significant difference with incubation time. At the concentration of 31.25 µg/mL, the loss of GSH activity is nearly 58% which increased to 89% at the concentration of 250 µg/mL and almost 90% at 500 µg/mL and 1000 µg/mL. The results show that when the concentration is increased beyond 250 µg/mL, there is no significant change in the loss of GSH (Figure 8a). Therefore, 250 µg/mL is the minimum concentration most effectively reducing the GSH activity. The above results agree well with the growth kinetics study of both bacteria. Also, from Fig. 8b, it is visible that there is no significant loss in GSH with time, suggesting that 2 hrs incubation time is enough to oxidize GSH. The strong oxidation of GSH by the MoS₂-cys NFs supports that the NFs can oxidize thiols or other cellular components, consequently killing the bacteria by interfering with their defense mechanism. Therefore, it is clear from the above results that the MoS₂-cys NFs can generate significant ROS-independent oxidative stress. Thus, from the above results, we see that the antibacterial mechanism of MoS₂-cys NFs is due to the combined effect of ROS-independent and ROS-dependent oxidative stress. Thus, from

the above results and report findings, we propose that the large interaction sites over the surface of NFs and the thin dimension of NSs in the form of petals are capable of generating oxidative stresses and membrane destruction, leading to the death of the bacteria.

3.4. Cellular toxicity studies:

Fig. 9 shows the MTT assay evaluated cellular toxicity of MoS₂-cys NFs against the HFF cell line. The HFF cells were treated with different concentrations of MoS₂-cys NFs. Analysis of the results showed that after 48 hours of treatment with MoS₂-cys NFs, there was a minimal/non-significant decrease in cell viability at doses up to 250 µg/mL. It has been observed that, on average, 90% of cells are still viable after treatment. These results suggest that MoS₂-cys NFs cause negligible toxicity to eukaryotic cells. This finding implies that the nanoflower's safety and cytotoxicity profiles are within acceptable limits under normal *in-vitro* experimental conditions. It could be used as a non-toxic material for further research.

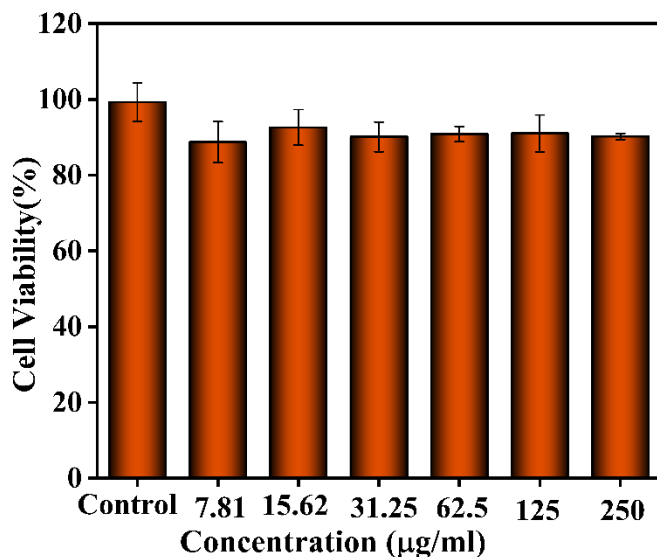


Figure 9. In-vitro cytotoxicity study of MoS₂-cys NFs. % Cell viability was assessed by MTT assay with varying concentrations. The cell viability of control cells was taken as 100%. The data shown are the mean ± SD (n=3).

4. Conclusions:

MoS₂-cys NFs were successfully synthesized using the simple hydrothermal method. Various characterizing techniques confirm the formation of cysteine-capped MoS₂ NFs. XRD confirmed the formation of 2H-phase and purity of MoS₂-cys NFs, and FE-SEM and TEM confirmed the size and flower-like morphology. The XPS also confirms the formation of MoS₂ and the surface modification with L-cysteine. FTIR further confirms the presence of L-cysteine, and DTA-TGA analysis estimates 18% L-cysteine over the surface. Moreover, the as-prepared NFs have also demonstrated very high colloidal stability in aqueous solutions throughout the experimental conditions with only nearly 3% aggregation in 24 hrs. Further, the antibacterial studies using the broth dilution method against both gram-negative and gram-positive bacterial strains revealed the high potential of these NFs in inhibiting their growth in a concentration and time-dependent manner. The incubation of 250 µg/mL of MoS₂-cys NFs with *E. coli* and *S. aureus*, respectively, for 6 hrs have shown more than 90% inhibition of both bacterial strains, confirming their potency as antibacterial agents. Moreover, the antibacterial mechanisms insights suggest that the presence of more interaction sites and thin dimension of nanosheets in MoS₂-cys NFs results in enhanced antibacterial activity. This enhancement is due to combined effect of membrane damage, ROS-dependent and, ROS-independent oxidative stresses. Furthermore, toxicity studies of MoS₂-cys NFs confirm the high biocompatibility of as-prepared NFs.

The antibacterial activity of non-toxic MoS₂-cys NFs suggests their future biomedical applications, such as wound healing, water disinfection, antibacterial coatings, and in textile and food industries. Additionally, due to the inherent photothermal property of MoS₂, our future study aims to investigate the potential enhancement of antibacterial efficiency of MoS₂-cys NFs upon light exposure. Moreover, due to the high biocompatibility and colloidal stability of the MoS₂-cys NFs,

they may be used as a drug carrier in treating diseases like, cancer. Apart from biomedical applications, due to the greater surface area and active edges, the as-prepared nanostructures could be used in catalysis, sensing, supercapacitors, solar cells, hydrogen evolution applications, etc.

Conflicts of interest:

The authors declare no conflicts of interest.

Acknowledgments:

RK acknowledges the Ministry of Human Resource and Development, India, for the fellowship. ANG acknowledges the financial support from the Department of Science and Technology, India, grant no. CRG/2019/001684. We thank the central research facility for the XRD, FE-SEM, TEM, XPS, FTIR, and TGA measurements. The authors highly acknowledge the support provided by the SERB Department of Science and Technology, Govt. of India (JCB/2019/000008), and Indian Council of Medical Research (ICMR) (Sanction Letter No: 5/13/53/2020-NCD-III

References:

- (1) de Kraker, M. E. A.; Stewardson, A. J.; Harbarth, S. Will 10 Million People Die a Year Due to Antimicrobial Resistance by 2050? *PLoS Med* **2016**, *13* (11), e1002184. <https://doi.org/10.1371/JOURNAL.PMED.1002184>.
- (2) Cosgrove, S. E.; Sakoulas, G.; Perencevich, E. N.; Schwaber, M. J.; Karchmer, A. W.; Carmeli, Y. Comparison of Mortality Associated with Methicillin-Resistant and Methicillin-Susceptible *Staphylococcus Aureus* Bacteremia: A Meta-Analysis. *Clinical Infectious Diseases* **2003**, *36*, 53–62.
- (3) McKenna, M. The Last Resort: Health Officials Are Watching in Horror as Bacteria Become Resistant to Powerful Carbapenem Antibiotics--One of the Last Drugs on the Shelf. *Nature* **2013**, *499* (7459), 394–397.
- (4) Allahverdiyev, A. M.; Kon, K. V.; Abamor, E. S.; Bagirova, M.; Rafailovich, M. Coping with Antibiotic Resistance: Combining Nanoparticles with Antibiotics and Other Antimicrobial Agents. *Expert Rev Anti Infect Ther* **2011**, *9* (11), 1035–1052. <https://doi.org/10.1586/ERI.11.121>.

- (5) Lee, N. Y.; Ko, W. C.; Hsueh, P. R. Nanoparticles in the Treatment of Infections Caused by Multidrug-Resistant Organisms. *Front Pharmacol* **2019**, *10*, 1153. <https://doi.org/10.3389/FPHAR.2019.01153/BIBTEX>.
- (6) Deshmukh, S. P.; Patil, S. M.; Mullani, S. B.; Delekar, S. D. Silver Nanoparticles as an Effective Disinfectant: A Review. *Materials Science and Engineering: C* **2019**, *97*, 954–965. <https://doi.org/10.1016/J.MSEC.2018.12.102>.
- (7) Gaillet, S.; Rouanet, J. M. Silver Nanoparticles: Their Potential Toxic Effects after Oral Exposure and Underlying Mechanisms--a Review. *Food Chem Toxicol* **2015**, *77*, 58–63. <https://doi.org/10.1016/J.FCT.2014.12.019>.
- (8) Li, X.; Robinson, S. M.; Gupta, A.; Saha, K.; Jiang, Z.; Moyano, D. F.; Sahar, A.; Riley, M. A.; Rotello, V. M. Functional Gold Nanoparticles as Potent Antimicrobial Agents against Multi-Drug-Resistant Bacteria. *ACS Nano* **2014**, *8* (10), 10682–10686. https://doi.org/10.1021/NN5042625/SUPPL_FILE/NN5042625_SI_001.PDF.
- (9) Gokce, C.; Gurcan, C.; Besbinar, O.; Unal, M. A.; Yilmazer, A. Emerging 2D Materials for Antimicrobial Applications in the Pre- and Post-Pandemic Era. *Nanoscale* **2022**, *14* (2), 239–249. <https://doi.org/10.1039/D1NR06476B>.
- (10) Lu, J.; Chen, M.; Dong, L.; Cai, L.; Zhao, M.; Wang, Q.; Li, J. Molybdenum Disulfide Nanosheets: From Exfoliation Preparation to Biosensing and Cancer Therapy Applications. *Colloids Surf B Biointerfaces* **2020**, *194*, 111162. <https://doi.org/10.1016/J.COLSURFB.2020.111162>.
- (11) Yadav, V.; Roy, S.; Singh, P.; Khan, Z.; Jaiswal, A.; Yadav, V.; Roy, S.; Singh, P.; Jaiswal, A.; Khan, Z. 803706 (1 of 33) 2D MoS₂-Based Nanomaterials for Therapeutic, Bioimaging, and Biosensing Applications. **2018**. <https://doi.org/10.1002/sml.201803706>.
- (12) Sethulekshmi, A. S.; Saritha, A.; Joseph, K.; Aprem, A. S.; Sisupal, S. B. MoS₂ Based Nanomaterials: Advanced Antibacterial Agents for Future. *Journal of Controlled Release* **2022**, *348*, 158–185. <https://doi.org/10.1016/J.JCONREL.2022.05.047>.
- (13) Yang, X.; Li, J.; Liang, T.; Ma, C.; Zhang, Y.; Chen, H.; Hanagata, N.; Su, H.; Xu, M. Antibacterial Activity of Two-Dimensional MoS₂ Sheets †. **2014**. <https://doi.org/10.1039/c4nr01965b>.
- (14) Ma, Y.; Xu, H.; Shen, X.; Pang, Y. Facile Photoreductive Synthesis of Silver Nanoparticles for Antimicrobial Studies. *Advanced Powder Technology* **2021**, *32* (6), 2116–2121. <https://doi.org/10.1016/J.APT.2021.04.024>.
- (15) Sidhu, A. K.; Verma, N.; Kaushal, P. Role of Biogenic Capping Agents in the Synthesis of Metallic Nanoparticles and Evaluation of Their Therapeutic Potential. *Frontiers in Nanotechnology* **2022**, *3*, 105. <https://doi.org/10.3389/FNANO.2021.801620/BIBTEX>.
- (16) Tiwari, S.; Gupta, P. K.; Bagbi, Y.; Sarkar, T.; Solanki, P. R. L-Cysteine Capped Lanthanum Hydroxide Nanostructures for Non-Invasive Detection of Oral Cancer Biomarker. *Biosens Bioelectron* **2017**, *89*, 1042–1052. <https://doi.org/10.1016/J.BIOS.2016.10.020>.

- (17) Li, M.; Zhou, H.; Zhang, H.; Sun, P.; Yi, K.; Wang, M.; Dong, Z.; Xu, S. Preparation and Purification of L-Cysteine Capped CdTe Quantum Dots and Its Self-Recovery of Degenerate Fluorescence. *J Lumin* **2010**, *130* (10), 1935–1940. <https://doi.org/10.1016/J.JLUMIN.2010.05.008>.
- (18) Li, Y.; Chen, J.; Zhu, C.; Wang, L.; Zhao, D.; Zhuo, S.; Wu, Y. Preparation and Application of Cysteine-Capped ZnS Nanoparticles as Fluorescence Probe in the Determination of Nucleic Acids. *Spectrochim Acta A Mol Biomol Spectrosc* **2004**, *60* (8–9), 1719–1724. <https://doi.org/10.1016/J.SAA.2003.09.012>.
- (19) Zuo, F.; Yan, S.; Zhang, B.; Zhao, Y.; Xie, Y. L-Cysteine-Assisted Synthesis of PbS Nanocube-Based Pagoda-like Hierarchical Architectures. **2008**. <https://doi.org/10.1021/jp0766149>.
- (20) Sharma, B.; Rabinal, M. K. Biologically Active L-Cysteine as a Reducing/Capping Agent for Controlled Tuning of Gold Nanoparticles. *J Alloys Compd* **2015**, *649*, 11–18. <https://doi.org/10.1016/J.JALLCOM.2015.06.160>.
- (21) Sharifi, E.; Shams, E.; Salimi, A.; Noorbakhsh, A.; Amini, M. K. Nickel-Cysteine Nanoparticles: Synthesis, Characterization and Application for Direct Electron Transfer Studies. *Colloids Surf B Biointerfaces* **2018**, *165*, 135–143. <https://doi.org/10.1016/J.COLSURFB.2018.01.052>.
- (22) Mulu, M.; RamaDevi, D.; Belachew, N.; Basavaiah, K. Hydrothermal Green Synthesis of MoS₂ Nanosheets for Pollution Abatement and Antifungal Applications. *RSC Adv* **2021**, *11* (40), 24536–24542. <https://doi.org/10.1039/D1RA03815J>.
- (23) Hariharan, S.; Karthikeyan, B. Optical and Surface Band Bending Mediated Fluorescence Sensing Properties of MoS₂ Quantum Dots †. **2016**. <https://doi.org/10.1039/c6ra21157g>.
- (24) Ding, L.; Chang, Y.; Yang, P.; Gao, W.; Sun, M.; Bie, Y.; Yang, L.; Ma, X.; Guo, Y. Facile Synthesis of Biocompatible L-Cysteine-Modified MoS₂ Nanospheres with High Photothermal Conversion Efficiency for Photothermal Therapy of Tumor. *Materials Science and Engineering: C* **2020**, *117*, 111371. <https://doi.org/10.1016/J.MSEC.2020.111371>.
- (25) Xu, Q. B.; Gu, J. Y.; Zhao, Y.; Ke, X. T.; Liu, X. D. Antibacterial Cotton Fabric with Enhanced Durability Prepared Using L-Cysteine and Silver Nanoparticles. *Fibers and Polymers* **2017**, *18* (11), 2204–2211. <https://doi.org/10.1007/S12221-017-7567-Z/METRICS>.
- (26) Xu, Q.; Duan, P.; Zhang, Y.; Fu, F.; Liu, X. Double Protect Copper Nanoparticles Loaded on L-Cysteine Modified Cotton Fabric with Durable Antibacterial Properties. *Fibers and Polymers* **2018**, *19* (11), 2324–2334. <https://doi.org/10.1007/s12221-018-8621-1>.
- (27) Wang, H.; Qian, J.; Gu, J.; Yan, W.; Zhang, J. Steric Configuration-Enabled Selective Antimicrobial Activity of Chiral Cysteine. *Biochem Biophys Res Commun* **2019**, *512* (3), 505–510. <https://doi.org/10.1016/J.BBRC.2019.03.080>.
- (28) Karunakaran, S.; Pandit, S.; Basu, B.; De, M. Simultaneous Exfoliation and Functionalization of 2H-MoS₂ by Thiolated Surfactants: Applications in Enhanced Antibacterial Activity. *J. Am. Chem. Soc* **2018**, *140*, 12634–12644. <https://doi.org/10.1021/jacs.8b08994>.
- (29) Pandit, S.; Karunakaran, S.; Kumar Boda, S.; Basu, B.; De, M. High Antibacterial Activity of Functionalized Chemically Exfoliated MoS₂. **2016**. <https://doi.org/10.1021/acsami.6b10916>.

- (30) Rajab Ali, S.; De, M. Fe-Doped MoS₂ Nanozyme for Antibacterial Activity and Detoxification of Mustard Gas Simulant. *Cite This: ACS Appl. Mater. Interfaces* **2022**, *14*, 42940–42949. <https://doi.org/10.1021/acscami.2c11245>.
- (31) Wang, P.; Wang, H.; Zhao, X.; Li, L.; Chen, M.; Cheng, J.; Liu, J.; Li, X. Antibacterial Activity and Cytotoxicity of Novel Silkworm-like Nisin@PEGylated MoS₂. *Colloids Surf B Biointerfaces* **2019**, *183*. <https://doi.org/10.1016/j.colsurfb.2019.110491>.
- (32) Antibiotic-Loaded MoS₂ Nanosheets to Combat Bacterial Resistance via Biofilm Inhibition. **2017**. <https://doi.org/10.1088/1361-6528/aa6c9b>.
- (33) Cao, F.; Ju, E.; Zhang, Y.; Wang, Z.; Liu, C.; Li, W.; Huang, Y.; Dong, K.; Ren, J.; Qu, X. An Efficient and Benign Antimicrobial Depot Based on Silver-Infused MoS₂. **2017**. <https://doi.org/10.1021/acsnano.7b00343>.
- (34) Yan, H.; Liu, L.; Wang, R.; Zhu, W.; Ren, X.; Luo, L.; Zhang, X.; Luo, S.; Ai, X.; Wang, J. Binary Composite MoS₂/TiO₂ Nanotube Arrays as a Recyclable and Efficient Photocatalyst for Solar Water Disinfection. **2020**. <https://doi.org/10.1016/j.cej.2020.126052>.
- (35) Awasthi, G. P.; Adhikari, S. P.; Ko, S.; Kim, H. J.; Park, C. H.; Kim, C. S. Facile Synthesis of ZnO Flowers Modified Graphene like MoS₂ Sheets for Enhanced Visible-Light-Driven Photocatalytic Activity and Antibacterial Properties. *J Alloys Compd* **2016**, *682*, 208–215. <https://doi.org/10.1016/j.jallcom.2016.04.267>.
- (36) Yin, W.; Yu, J.; Lv, F.; Yan, L.; Rong Zheng, L.; Gu, Z.; Zhao, Y. Functionalized Nano-MoS₂ with Peroxidase Catalytic and Near-Infrared Photothermal Activities for Safe and Synergetic Wound Antibacterial Applications Including V₂O₅, 11 Fe₃O₄, 12 and Graphene Quantum Dots, 20 Have the Peroxidase-Mimic Ability and Can Be Used to Assist H₂O₂ for Antibacterial. *ACS Nano* **2016**, *10*, 11000–11011. <https://doi.org/10.1021/acsnano.6b05810>.
- (37) Zhao, X.; Chen, M.; Wang, H.; Xia, L.; Guo, M.; Jiang, S.; Wang, Q.; Li, X.; Yang, X. Synergistic Antibacterial Activity of Streptomycin Sulfate Loaded PEG-MoS₂/RGO Nanoflakes Assisted with near-Infrared. **2020**. <https://doi.org/10.1016/j.msec.2020.111221>.
- (38) Zhang, M.; Wang, K.; Zeng, S.; Xu, Y.; Nie, W.; Chen, P.; Zhou, Y. Visible Light-Induced Antibacterial Effect of MoS₂: Effect of the Synthesis Methods. *Chemical Engineering Journal* **2021**, *411*, 128517. <https://doi.org/10.1016/j.cej.2021.128517>.
- (39) Cao, W.; Yue, L.; Zhang, Y.; Wang, Z. Photodynamic Chitosan Functionalized MoS₂ Nanocomposite with Enhanced and Broad-Spectrum Antibacterial Activity. *Carbohydr Polym* **2022**, *277*, 144–8617. <https://doi.org/10.1016/j.carbpol.2021.118808>.
- (40) Kumar, P.; Roy, S.; Sarkar, A.; Jaiswal, A. Reusable MoS₂-Modified Antibacterial Fabrics with Photothermal Disinfection Properties for Repurposing of Personal Protective Masks. *ACS Appl Mater Interfaces* **2021**, *13* (11), 12912–12927. https://doi.org/10.1021/ACSAMI.1C00083/ASSET/IMAGES/MEDIUM/AM1C00083_M004.GIF.

- (41) Bezza, F. A.; Tichapondwa, S. M.; Chirwa, M. N. Fabrication of Monodispersed Copper Oxide Nanoparticles with Potential Application as Antimicrobial Agents. *Scientific Reports* | **123AD**, *10*, 16680. <https://doi.org/10.1038/s41598-020-73497-z>.
- (42) Xu, Q.; Zhu, P.; Zhang, J.; Liu, Y.; Cai, L.; Jiang, H.; Ji, M.; Chen, J. Electrochemical Formation of Distinct Nanostructured MoS₂ with Altered Antibacterial Activity. *Mater Lett* **2020**, *271*, 127809. <https://doi.org/10.1016/J.MATLET.2020.127809>.
- (43) Yang, X.; Li, J.; Liang, T.; Ma, C.; Zhang, Y.; Chen, H.; Hanagata, N.; Su, H.; Xu, M. Antibacterial Activity of Two-Dimensional MoS₂ Sheets †. **2014**. <https://doi.org/10.1039/c4nr01965b>.
- (44) De, D.; Chandan, K.; Das, D.; Mandal, M.; Mandal, N.; Pawar, A.; Chandra, A.; Nath, G. Curcumin Complexed with Graphene Derivative for Breast Cancer Therapy. **2020**. <https://doi.org/10.1021/acsabm.0c00771>.
- (45) Eda, G.; Yamaguchi, H.; Voiry, D.; Fujita, T.; Chen, M.; Chhowalla, M. Photoluminescence from Chemically Exfoliated MoS₂. *Nano Lett* **2011**, *11*, 5111–5116. <https://doi.org/10.1021/nl201874w>.
- (46) Kasinathan, K.; Murugesan, B.; Pandian, N.; Mahalingam, S.; Selvaraj, B.; Marimuthu, K. Synthesis of Biogenic Chitosan-Functionalized 2D Layered MoS₂ Hybrid Nanocomposite and Its Performance in Pharmaceutical Applications: In-Vitro Antibacterial and Anticancer Activity. *Int J Biol Macromol* **2020**, *149*, 1019–1033. <https://doi.org/10.1016/J.IJBIOMAC.2020.02.003>.
- (47) Mishra, H.; Singh, V. K.; Ali, R.; Vikram, K.; Singh, J.; Misra, A.; Mishra, H.; Srivastava, A. Fluorescence Quenching of Molybdenum Disulfide Quantum Dots for Metal Ion Sensing. **2020**, *151*, 729–741. <https://doi.org/10.1007/s00706-020-02598-2>.
- (48) Aryal, S.; Remant, B. K. C.; Dharmaraj, N.; Bhattarai, N.; Kim, C. H.; Kim, H. Y. Spectroscopic Identification of SAu Interaction in Cysteine Capped Gold Nanoparticles. *Spectrochim Acta A Mol Biomol Spectrosc* **2006**, *63* (1), 160–163. <https://doi.org/10.1016/J.SAA.2005.04.048>.
- (49) Kogelheide, F.; Kartaschew, K.; Strack, M.; Baldus, S.; Metzler-Nolte, N.; Havenith, M.; Awakowicz, P.; Stapelmann, K.; Lackmann, J. W. FTIR Spectroscopy of Cysteine as a Ready-to-Use Method for the Investigation of Plasma-Induced Chemical Modifications of Macromolecules. *J Phys D Appl Phys* **2016**, *49* (8), 084004. <https://doi.org/10.1088/0022-3727/49/8/084004>.
- (50) Roy, S.; Mondal, A.; Yadav, V.; Sarkar, A.; Banerjee, R.; Sanpui, P.; Jaiswal, A. Mechanistic Insight into the Antibacterial Activity of Chitosan Exfoliated MoS₂ Nanosheets: Membrane Damage, Metabolic Inactivation, and Oxidative Stress. **2019**. <https://doi.org/10.1021/acsabm.9b00124>.
- (51) Mutalik, C.; Ika Krisnawati, D.; Patil, S. B.; Khafid, M.; Susetiyanto Atmojo, D.; Santoso, P.; Lu, S.-C.; Wang, D.-Y.; Kuo, T.-R. Phase-Dependent MoS₂ Nanoflowers for Light-Driven Antibacterial Application. **2021**. <https://doi.org/10.1021/acssuschemeng.1c01868>.
- (52) Tian, X.; Sun, Y.; Fan, S.; Boudreau, M. D.; Chen, C.; Ge, C.; Yin, J. J. Photogenerated Charge Carriers in Molybdenum Disulfide Quantum Dots with Enhanced Antibacterial Activity. *ACS Appl Mater Interfaces* **2019**, *11* (5), 4858–4866. https://doi.org/10.1021/ACSAMI.8B19958/SUPPL_FILE/AM8B19958_SI_001.PDF.

- (53) Mondal, A.; De, M. Amino Acid-Functionalized MoS₂ Quantum Dots for Selective Antibacterial Activity. *Cite This: ACS Appl. Nano Mater* **2021**. <https://doi.org/10.1021/acsanm.1c03243>.
- (54) Dong, S. M.; Li, J.; Liu, L.; Wu, R.; Ou, X.; Tian, R.; Zhang, J.; Jin, H.; Dong, M. Membrane Destruction and Phospholipid Extraction by Using Two-Dimensional MoS₂ Nanosheets †. *Nanoscale* **2018**, *10*. <https://doi.org/10.1039/c8nr04207a>.
- (55) Simon, H.-U.; Haj-Yehia, A.; Levi-Schaffer, F. Role of Reactive Oxygen Species (ROS) in Apoptosis Induction. *Apoptosis* **2000**, *5*, 415–418.
- (56) Thannickal, V. J.; Fanburg, B. L. Downloaded from Journals.Physiology.Org/Journal/Ajplung. *Am J Physiol Lung Cell Mol Physiol* **2000**, *279*, 1005–1028.
- (57) Xiong, Z.; Zhang, X.; Zhang, S.; Lei, L.; Ma, W.; Li, D.; Wang, W.; Zhao, Q.; Xing, B. Bacterial Toxicity of Exfoliated Black Phosphorus Nanosheets. *Ecotoxicol Environ Saf* **2018**, *161*, 507–514. <https://doi.org/10.1016/J.ECOENV.2018.06.008>.
- (58) Fahey, R. C.; Brown, W. C.; Adams, W. B.; Worsham, M. B. Occurrence of Glutathione in Bacteria. *J Bacteriol* **1978**, *133* (3), 1126–1129. <https://doi.org/10.1128/JB.133.3.1126-1129.1978>.

Graphical Abstract

